Microstructure and enhanced cryogenic tensile property of a heterostructured Al–AlN/Al–Mg composite fabricated by accumulative roll bonding (ARB)

Article *in* Journal of Materials Research and Technology · September 2022

DOI: 10.1016/j.jmrt.2022.09.037

CITATIONS
21

READS
125

8 authors, including:

Jinfeng Nie
Nanjing University of Science and Technology
89 PUBLICATIONS **2,047** CITATIONS
SEE PROFILE

Yong Fan
Nanjing University of Science and Technology
13 PUBLICATIONS **137** CITATIONS
SEE PROFILE

Sida Liu
Xi'an Jiaotong University
58 PUBLICATIONS **803** CITATIONS
SEE PROFILE

Xiangfa Liu
Shandong University
368 PUBLICATIONS **8,113** CITATIONS
SEE PROFILE

Available online at www.sciencedirect.com

jmr&t Journal of Materials Research and Technology

journal homepage: www.elsevier.com/locate/jmrt

Original Article

Microstructure and enhanced cryogenic tensile property of a heterostructured Al–AlN/Al–Mg composite fabricated by accumulative roll bonding (ARB)

Xinda Sun [a,1], *Xiaojie Hao* [a,1], *Jinfeng Nie* [a,*], *Yong Fan* [a], *Yuyao Chen* [a], *Sida Liu* [b], *Xiangfa Liu* [c], *Yonghao Zhao* [a,**]

[a] *Nano and Heterogeneous Materials Center, School of Materials Science and Engineering, Nanjing University of Science and Technology, Nanjing 210094, China*

[b] *Institute for Advanced Technology, Shandong University, Jinan 250061, China*

[c] *Key Laboratory for Liquid–Solid Structural Evolution and Processing of Materials, Ministry of Education, Shandong University, Jinan 250061, China*

ARTICLE INFO

Article history:
Received 2 August 2022
Accepted 8 September 2022
Available online 13 September 2022

Keywords:
Aluminum alloys
Accumulative roll-bonding
Laminated composites
Heterogeneous structure
Hetero-deformation induced hardening

ABSTRACT

Recently, heterogeneous structured materials have attracted considerable attention due to their excellent mechanical properties. In this work, a heterostructured Al–AlN/Al–Mg laminated composite was successfully prepared by accumulative roll-bonding (ARB), and the microstructural evolution and tensile properties both at room temperature and under liquid nitrogen temperature were investigated systematically. It is found that the distribution of AlN particles in Al–AlN layer has been optimized to be more uniform to avoid sever stress concentration; both the Al matrix grains in the Al–AlN and Al–Mg layers were refined significantly with the increase of ARB cycles. In addition, the interfaces of Al–AlN and Al–Mg layers were well bonded and kept straight without any necking or fracture after ARB process. Compared with the room temperature tensile properties, the cryogenic tensile strength, yield strength and ductility of the Al–AlN/Al–Mg composite under liquid nitrogen temperature were enhanced simultaneously, which reached to 473.7 MPa, 363.1 MPa and 9.88%, increased by 51.8%, 39.0% and 83.3%, respectively. It is found that the strain hardening rate under liquid nitrogen temperature was also enhanced significantly. It is proposed that the hetero-deformation induced (HDI) stress played a crucial role in the significant enhancement of tensile strength and ductility for the laminated composites.

* Corresponding author.
** Corresponding author.
E-mail addresses: niejinfeng@njust.edu.cn (J. Nie), yhzhao@njust.edu.cn (Y. Zhao).
[1] These authors contributed equally.

https://doi.org/10.1016/j.jmrt.2022.09.037

1. Introduction

The advance of science and technology puts forward a variety of higher performance requirements for service materials. However, these requirements cannot be readily met at the same time for materials with single phase or constituent. Laminated metal composites (LMCs), consisting of two or more metals, have been developed for their excellent mechanical properties, electrochemistry characteristics and corrosion resistance. Generally, strength and ductility are the two most important parameters of mechanical properties, especially for cryogenic structural applications. However, the two aspects are often exclusive of each other, i.e., a material may have the mechanical property of either high strength or good ductility, but rarely are both achieved simultaneously. Recently, heterogeneous structure design strategy is recognized to provide a feasible solution for increasing the strength and ductility synchronously [1–7]. Heterogeneous materials can be defined as a material with dramatic heterogeneity in strength or microstructure in different domains, which can be referred to as hard domain and soft domain, respectively [8,9]. During tensile deformation of heterogeneous materials, dislocation slip firstly started in the soft domain to produce plastic strain while the hard domain remains elastic. The soft domain needs to deform together with the adjacent hard domain, so there will be a plastic strain gradient in the soft domain near the domain interface [10,11]. In this elastic–plastic deformation stage, geometrically necessary dislocations (GNDs) will accumulate in the soft domain near the domain interface, which generates back stress in the soft domain and forward stress in the hard domain [12]. The back stress and the forward stress collectively produce the hetero-deformation induced (HDI) stress strengthening and extra strain hardening which simultaneously increase the strength and ductility of the heterogeneous material [13–18].

Recently, particle-reinforced aluminum matrix composites (PRAMCs) have received extensive attention due to their high temperature resistance, high specific strength and good wear resistance [19–21]. But there are very limited reports on the mechanical properties of PRAMCs at cryogenic environment. Lightweight aluminum alloys also show great potential for cryogenic applications [22,23]. It is reported that adding Mg to Al alloys can significantly improves the cryogenic tensile properties [24]. However, when both ceramic particles and Mg are added to the same Al matrix, Mg tends to enrich at the interface between the Al matrix and the reinforcement particle, and may result in the formation of harmful brittle phase, which may cause damage to the mechanical properties of the PRAMCs [25]. Accumulative roll-bonding (ARB) was firstly proposed by Saito and has been applied to prepare LMCs [26–29]. R. Jamaati et al. fabricated the Cu/Al_2O_3 [30] and Al/SiC [31] composites by distributing ceramic particles between metal sheets followed by ARB processing. However, the bonding between the particle and matrix was weak and a large number of pores were observed at low ARB cycles, which severely limited the properties of the composites. The matrix and ceramic particle of PRAMCs prepared by in-situ synthesis have high bonding strength, and their properties and structures are significantly different from those of alloys without particle reinforcement [32–35]. Therefore, rolling bonding in-situ synthesized PRAMCs and Al–Mg alloys will effectively avoid the negative interaction between Mg and ceramic particles and the weak bonding between the particle and matrix.

To improve the cryogenic mechanical properties of PRAMCs and provide some useful guidance for their cryogenic applications, a heterostructured Al–AlN/Al–Mg laminated composite with a sandwich structure was designed and fabricated by ARB up to three cycles. The Al–AlN nanocomposite prepared by liquid–solid in situ reaction was selected as one of laminated components, and the laminated structure were designed to improve the mechanical properties both at room temperature and cryogenic temperature. The Al–Mg plate was sandwiched between two Al–AlN plates. The microstructure evolution and mechanical properties at room temperature (RT) and liquid nitrogen temperature (LNT) of the heterostructured Al–AlN/Al–Mg laminated composites after different ARB cycles were systematically investigated. The

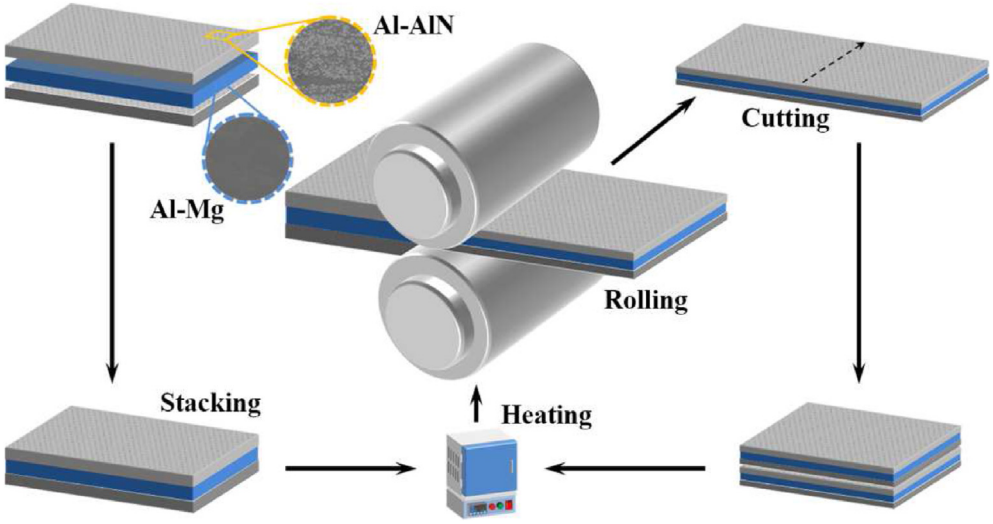

Fig. 1 – Diagrammatic illustration of the accumulative roll-bonding (ARB) process.

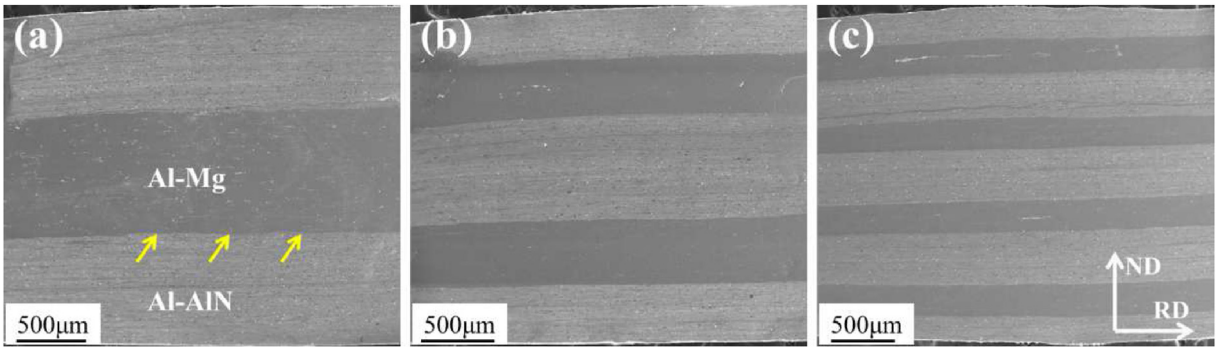

Fig. 2 – SEM micrographs of the Al–AlN/Al–Mg composite after (a) one; (b) two; (c) three cycles.

deformation mechanism and strengthening mechanism based on HDI stress were discussed in depth.

2. Experimental

2.1. Fabrication of the laminated composites

The raw materials used in this work are Al-8.2AlN composites and cast Al–5Mg alloy (all compositions quoted in this work are in wt.% unless otherwise stated). The as-received Al–AlN composites was fabricated according to the method reported in previous work [36], used commercial pure Al powders (99.7%), nitrogen plasmids powders (98.5%) and active carbon powders (99.0%) supplied by Shandong Al&Mg Melt Technology Co. Ltd. (Jinan, China) as raw material. The mass fraction of AlN was 8.2% and an extrusion ratio of 9:1 at 500 °C was selected. The Al–Mg ingot was treated at 380 °C for 2 h in a resistance furnace and then quenched in cold water.

The Al–AlN specimen and Al–Mg ingot were cut into sheets with sizes of 50 × 20 × 1.5 mm^3 and 50 × 20 × 2 mm^3, respectively, and then the Al–AlN and Al–Mg sheets were subjected to the ARB process. The schematic diagram of ARB process is shown in Fig. 1. The contact surface was degreased and decontaminated by acetone, wire brushed to provide a rough surface, and then the Al–Mg sheet was sandwiched between two Al–AlN sheets and the four corners were fixed with wire to achieve a good bonding between the sheets. The stacked sheets were preheated in a resistance furnace at 450 °C for 10 min and then rolled for 50% reduction in thickness without lubricant. Then the roll-bonded composite sheets were cut in half and stacked to their original thickness. The stacked sheets were preheated again at 450 °C and rolled with the same reduction, and then the same procedure was repeated up to three cycles.

2.2. Microstructure characterization and mechanical properties testing

The microstructures of the ARB processed specimens were characterized by a field emission scanning electron microscope (FESEM, Quanta 250F, FEI, Hillsboro, OR, USA) equipped with an energy dispersive spectroscopy (EDS, Oxford Instruments, Oxford, UK), electron back-scattered diffraction (EBSD, Zeiss, Jena, Thuringia, DE) and a transmission electron microscope (TEM, FEI, Hillsboro, USA). The samples for microstructure observation were etched with 0.5 vol.% hydrofluoric acid after mechanical polishing. The EBSD data was analyzed using the Channel 5 software.

The Vickers hardness test was carried out for fifteen times for the Al–AlN layer and Al–Mg layer of the laminated composites after different ARB cycles, respectively, on the rolling direction (RD)-normal direction (ND) plane using HMV-G 21DT at the load of 980.7 mN and held for 15 s. The tensile properties were determined using Walter + bai LFM 20 kN universal testing machine for uniaxial tensile testing at RT and LNT with the strain rate of 3 × 10^{-3} s^{-1}. The gauge size of the tensile test

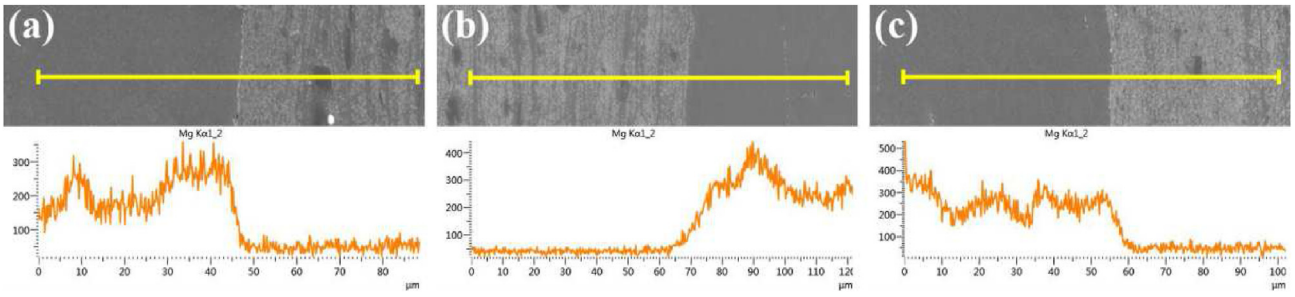

Fig. 3 – SEM micrograph and the EDS line-scanning analysis of the interface of Al–AlN/Al–Mg composite after (a) one; (b) two; (c) three cycles.

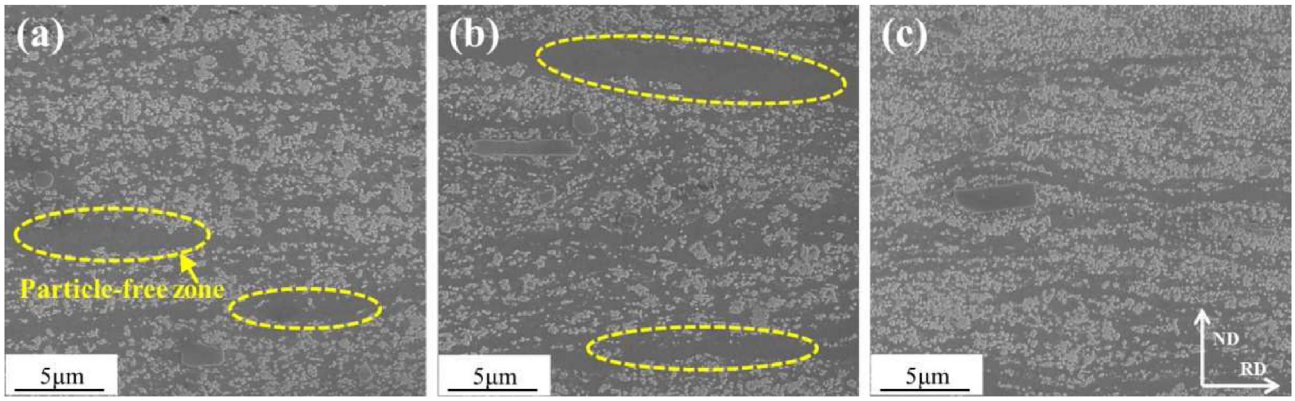

Fig. 4 – Particle distributions in Al–AlN layer after (a) one; (b) two; (c) three ARB cycles.

specimen was 10 mm in length and 2.5 mm in width, and the loading direction was parallel to the RD of the sheet.

3. Results

3.1. *Microstructure characterization of Al–AlN/Al–Mg laminated composite*

Fig. 2 shows the microstructure of the Al–AlN/Al–Mg composite on RD-ND plane after different ARB cycles. The interface between Al–AlN and Al–Mg layers was kept straight (indicated by the yellow arrow) during the whole rolling process and no obvious cracks were observed (Fig. 2a–c), indicating that the deformation of Al–AlN and Al–Mg layers was coordinated and a tight bonding between layers was achieved. Generally, the similar plastic flow behavior contributes to a good bonding between different sheets [37,38]. Therefore, it is supposed that the similar flow behavior of Al matrix and Al–Mg alloy resulted in a good metallurgical bonding at the interface during the ARB process. Moreover, the stacked sheet was preheated at 450 °C before rolling, which further improved its deformation ability and promoted a good deformation coordination of each layer.

To investigate the interface bonding quality of the composite, EDS line-scanning analysis were carried out. Fig. 3 shows the line-scanning spectrum of magnesium element across the interface between the Al–AlN and Al–Mg layers after different ARB cycles. As shown in Fig. 3a–c, a gradient distribution of elemental Mg was formed at the interface, indicating that Mg atoms in the Al–Mg layer diffused into the adjacent Al–AlN layer and then promoting the interlayer combination. Thus, it can prove that a tight metallurgical bonding between the Al–AlN and Al–Mg layers has been achieved through the atomic interdiffusion.

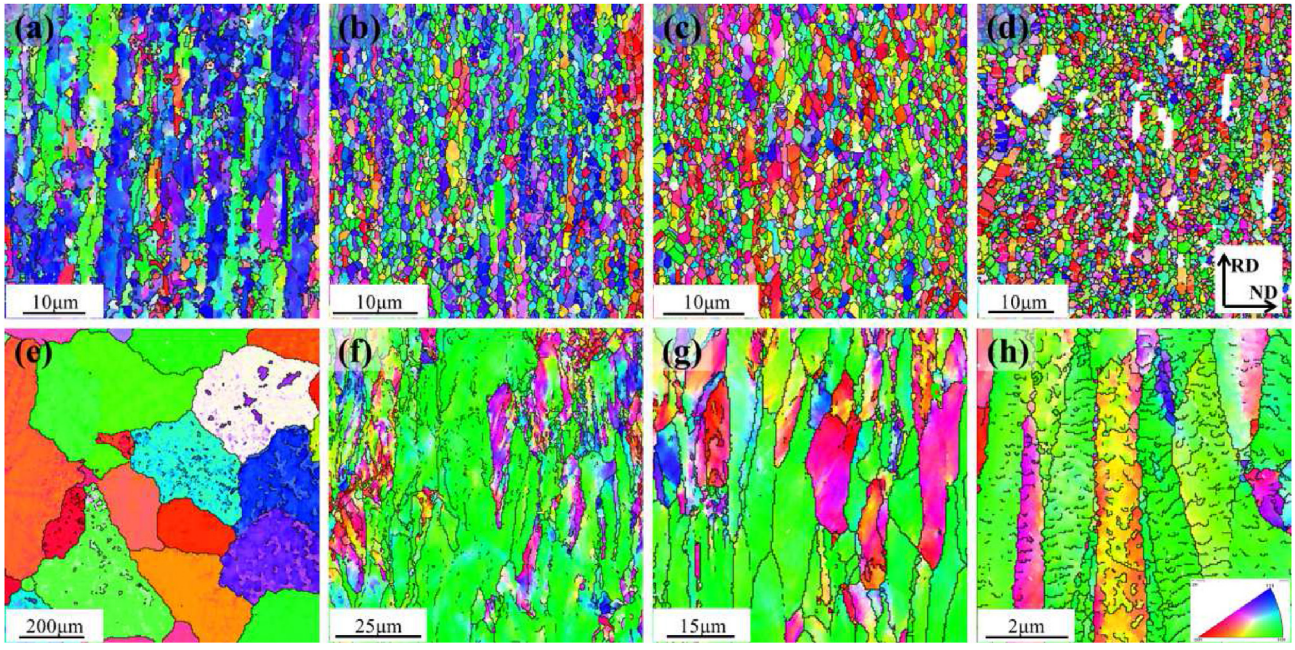

Fig. 5 – EBSD maps showing the matrix grain structure in Al–AlN layer (a–d) and Al–Mg layer (e–h) in the Al–AlN/Al–Mg composite before and after different ARB cycles: (a, e) as-received; (b, f) one; (c, g) two; (d, h) three cycles.

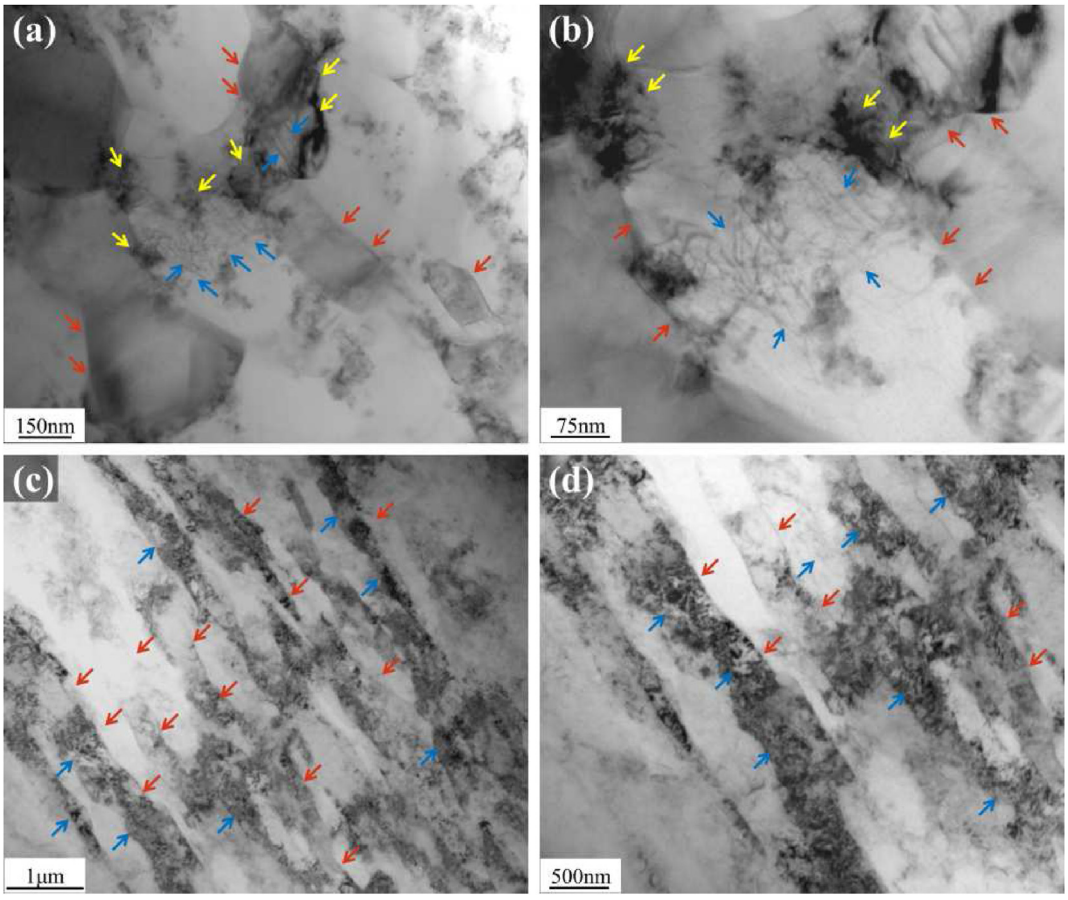

Fig. 6 – Typical TEM observation of the microstructure of the Al–AlN/Al–Mg composite after three ARB cycles: (a, b) Al–AlN layer; (c, d) Al–Mg layer.

It is expected that the rolling deformation can also influence the particle distribution in Al–AlN layer. Fig. 4 shows the AlN particle distribution in the Al–AlN layer. It can be seen that the AlN particle distributed inhomogeneously in the Al matrix and particle-free zones can be observed clearly after the first and second cycles (Fig. 4a and b). In addition, the size of particle-free zones was reduced and AlN particles became more uniformly distributed along the RD direction after three cycles. Therefore, the ARB process has promoted a more uniform distribution of AlN particles in the Al matrix along the rolling direction.

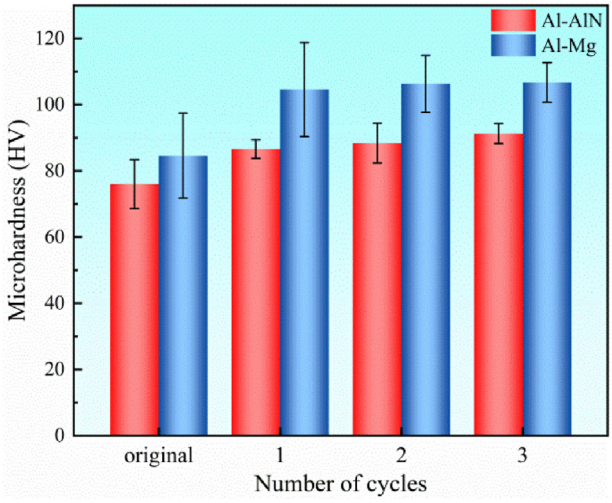

Fig. 7 – Microhardness of the Al–AlN/Al–Mg composite before and after different ARB cycles.

In order to evaluate the grain structure of aluminum matrix in the Al–AlN and Al–Mg layers after ARB processing, the EBSD maps of these samples on the RD-ND planes are shown in Fig. 5, respectively. As shown in Fig. 5a, most are elongated grains in the as-received Al–AlN layer and some equiaxed grains can also be seen, the average grain size is approximately ~1.88 μm. It is apparently that the Al grains were gradually refined to be equiaxed after the ARB processing, the average grain size was reduced to ~1.08 μm and ~0.99 μm after the first and second cycle (Fig. 5b and c), respectively. However, the average grain size was increased slightly to ~1.33 μm after the third cycle (Fig. 5d), which may be due to the accumulation of large strain within the material and the internal annealing during the ARB process promoting the recrystallization and grain growth occurred. Compared with the matrix grains in Al–AlN layer, the grains in the as-cast Al–Mg larger are much coarser. As shown in Fig. 5e, the as-received Al–Mg layer consists of coarse equiaxed Al grains with an average

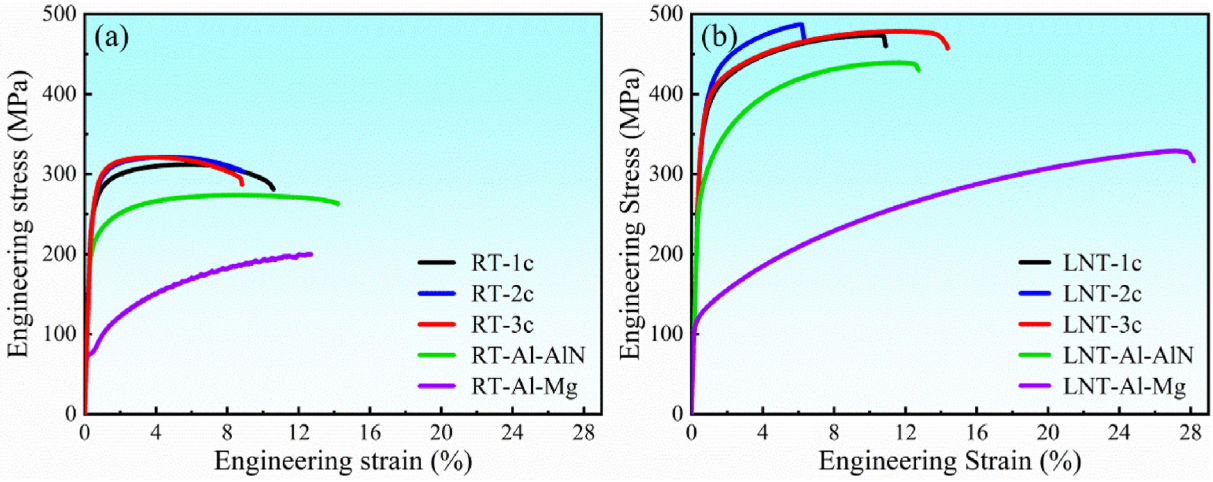

Fig. 8 – Engineering stress–strain curves of the Al–AlN/Al–Mg composite before and after ARB processing were tested at (a) RT and (b) LNT.

size of ~220 μm. After rolling deformation during the ARB processing, the Al grains were gradually elongated along RD and refined significantly as shown in Fig. 5f–h. Especially, the average elongated grain width was reduced to ~2.19 μm after three cycles, indicating that the matrix Al grains in the Al–Mg layer were also significantly refined after the large deformation strains.

In order to characterize the microstructure of the laminated composite at a higher magnification, TEM analysis was carried out to observe the distribution of particles and dislocations in the matrix after three ARB cycles. Fig. 6 shows the TEM images of the laminated composite after three cycles. As shown in Fig. 6a and b, the AlN particle (indicated by the yellow arrow) was mainly located at the grain boundaries (indicated by the red arrow) and there were a few aggregation areas inside the grains. Moreover, it can be observed that dislocations (indicated by the blue arrow) were tangled and accumulated in grains due to the pinning effect of AlN particles. As shown in Fig. 6c and d, the matrix grains of the Al–Mg layer were strip-shaped after three cycles, indicating that the continuously accumulated strain significantly changed the grain morphology. Meanwhile, a large number of dislocation walls and dislocation cells were also formed inside the grain as indicated by the blue arrow.

3.2. *Mechanical properties of Al–AlN/Al–Mg laminated composite*

The microhardness of the composite after different ARB cycles was shown in Fig. 7. The microhardness of Al–AlN and Al–Mg layers of the composite increased gradually with the increase of ARB cycles, and the microhardness value increased the most after the first cycle. The microhardness of Al–AlN and Al–Mg layers increased from 76.0 HV to 86.6 HV and 84.6 HV to 104.6 HV after the first ARB cycle, which increased by ~13% and ~23.6% compared with the original samples, respectively. Because the Al matrix grains in the as-cast Al–Mg were very coarse, thus the grain refinement effect was more obvious, and the dislocation generation and accumulation ability were stronger than those in the Al–AlN layer during ARB processing. Therefore, the increase of the microhardness value for the Al–Mg layer was higher than that of the Al–AlN layer after the first cycle. The increment of microhardness values decreases gradually in the following cycles, and the microhardness of Al–AlN and Al–Mg layers were increased to 91.3 HV and 106.7 HV after three ARB cycles, respectively. After the first cycle, the grain size was greatly reduced and a large number of dislocations were also generated, which contributed to a significant strength and hardness enhancement. Then the grain refinement rate and the dislocation accumulation capacity decreased with the further increase of ARB cycles, resulting in the reduction of work hardening. Therefore, the microhardness increment of the composites gradually decreased with the increased ARB cycles.

Fig. 8 shows the engineering stress–strain curves of the laminated composite tested at RT and LNT after different ARB cycles, and the details are given in Table 1 and Table 2. The RT ultimate tensile strength (UTS) and yield strength (YS) of the composite increased to ~ 312.1 MPa and ~261.3 MPa after the

Table 1 – Tensile properties of the laminated composite after different ARB cycles at RT.

Samples	YS/MPa	UTS/MPa	UE/%	EL/%
RT-1c	261.3	312.1	5.39	10.18
RT-2c	268.1	321.5	4.78	8.46
RT-3c	269.8	321.0	3.84	8.34
RT-Al-AlN	212.7	273.7	7.63	13.82
RT-Al-Mg	75.2	199.9	12.29	12.41

Table 2 – Tensile properties of the laminated composite after different ARB cycles at LNT.

Samples	YS/MPa	UTS/MPa	UE/%	EL/%
LNT-1c	363.1	473.7	9.88	10.19
LNT-2c	371.5	487.1	5.39	5.56
LNT-3c	370.7	478.6	12.10	13.73
LNT-Al-AlN	278.3	439.5	11.03	12.19
LNT-Al-Mg	119.1	328.9	26.68	27.55

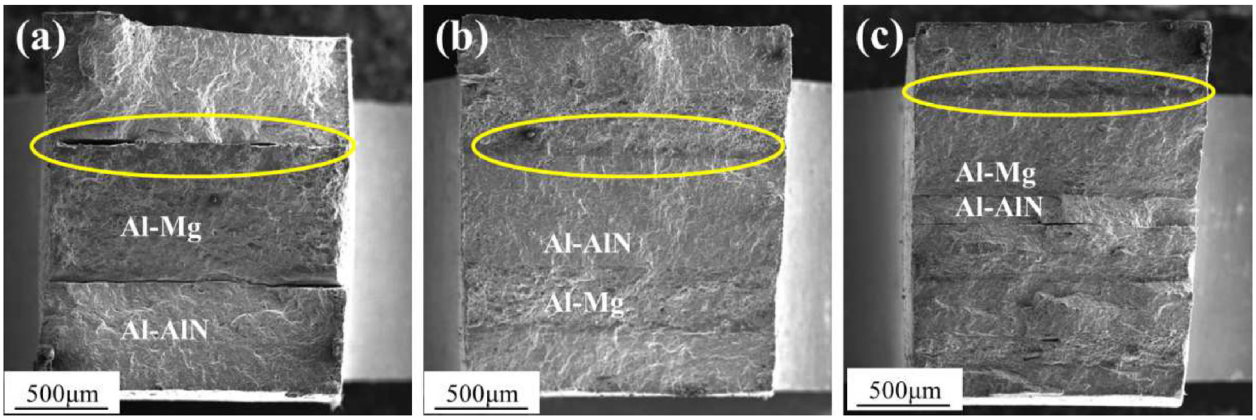

Fig. 9 – The RT tensile fracture surfaces of the laminated composite after ARB processing at lower magnification: (a) one; (b) two; (c) three cycles.

first ARB cycle, and maintained a good elongation to failure (EL) of ~10.18%. According to the role of the mixture:

$$\sigma_{ROM} = V_1\sigma_{Al-AlN} + V_2\sigma_{Al-Mg} \quad (1)$$

where $\sigma_{Al\text{-}AlN}$ and $\sigma_{Al\text{-}Mg}$ are UTS of as-received Al–AlN and as-cast Al–Mg sheets, respectively. V_1 and V_2 are the corresponding volume fractions, which are 0.6 and 0.4 for the composite after the first ARB cycle. σ_{ROM} is calculated to be about 244.2 MPa. The UTS of the composite after the first cycle was ~473.7 MPa at LNT and the corresponding σ_{ROM} is calculated to be about 395.3 MPa. Thus, it can be seen that the obtained UTS values of the composite after the first cycle both at RT and LNT is much higher than the calculated values according to the rule of mixture, indicating that the additional strengthening effect of the composite has been obtained by the heterogeneous laminated structure. A significant advantage of the heterogeneous laminated structure in terms of mechanical strengthening was shown. In addition, the tensile strength of the composites was increased with the increase of ARB cycles. Tables 1 and 2 show the statistics of UTS, YS, uniform elongation (UE) and EL of the composite after different ARB cycles. After the second ARB cycle, UTS and YS were further increased to ~321.5 MPa and ~268.1 MPa. However, after three ARB cycles, there was almost no change in strength and ductility compared to that after the second cycle. This may be due to the dynamic recovery and recrystallization that occurs during hot rolling, resulting in softening of the composite and thus offsetting the work hardening. The tensile strength and ductility measured at LNT showed the same trend as RT, and had higher strength and ductility

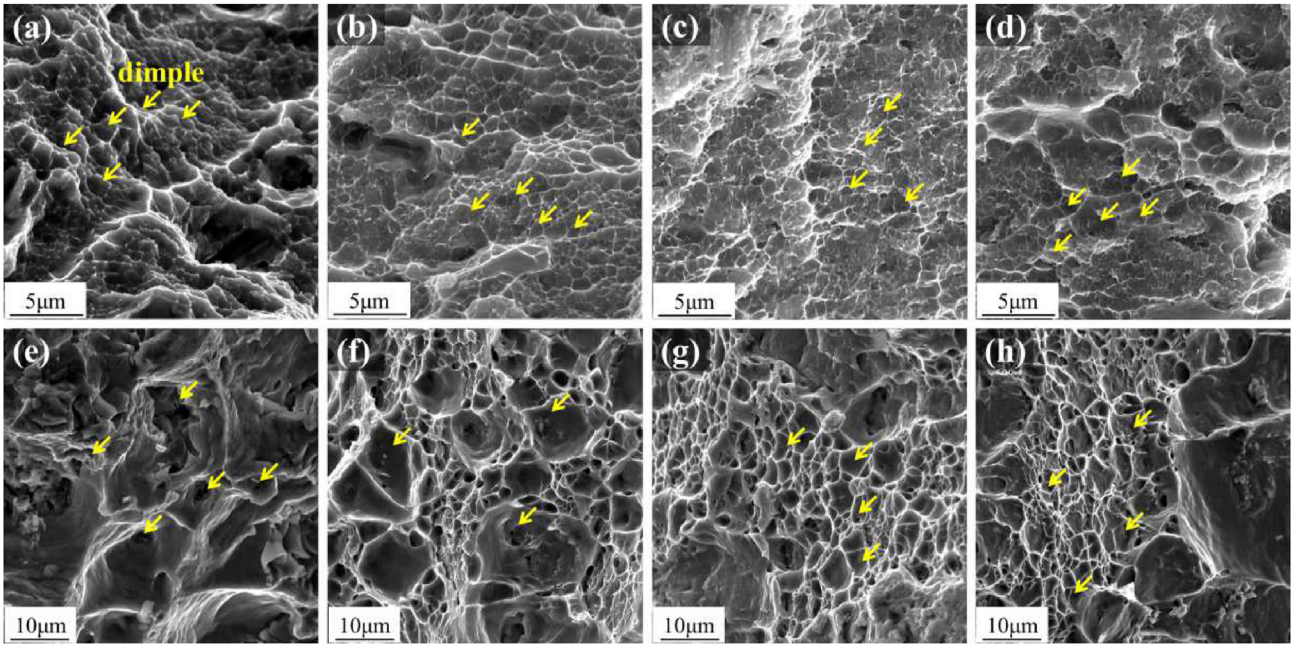

Fig. 10 – The RT tensile fracture surfaces of Al–AlN layer (a–d) and Al–Mg layer (e–h) in the laminated composite at higher magnification: (a, e) as-received; (b, f) one; (c, g) two; (d, h) three cycles.

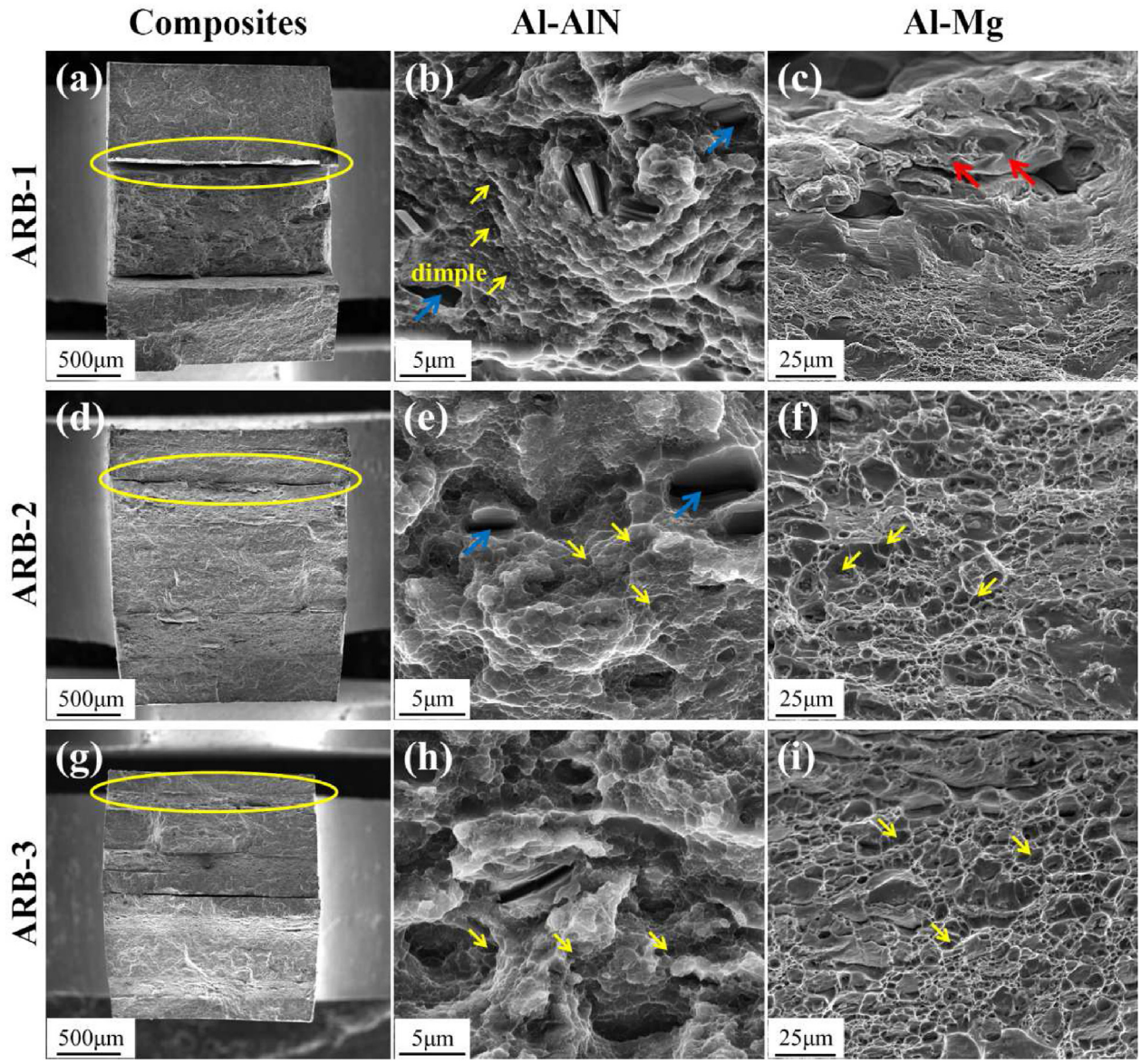

Fig. 11 – The LNT tensile fracture surfaces of the composite (a, d and g), Al–AlN layer (b, e and h) and Al–Mg layer (c, f and i): (a–c) one; (d–f) two; (g–i) three cycles.

combination compared with those obtained at RT. The UTS and EL of the composite after three ARB cycles were ~478.6 MPa and 13.73% at LNT, showing a superior strength and ductility synergy.

3.3. *Tensile fracture surfaces of Al–AlN/Al–Mg laminated composite*

In order to reveal the fracture mechanism and interface bonding strength, the tensile fracture surfaces of the different samples were analyzed. Fig. 9 shows the RT tensile fracture morphologies of the composites after different ARB cycles at lower magnification. As shown in Fig. 9a, it can be seen that discontinuous cracks distributed at the interface on the fracture surface for the composite after the first ARB cycle. This is due to the low bonding strength at the early stage of ARB and the difference in plastic deformation behaviors of Al–AlN and Al–Mg resulting in interlayer cracking. It is interesting to note that no obvious crack was found at the interfaces throughout the whole surface after the second and third ARB cycle (Fig. 9b and c), indicating that the bonding strength and synergistic deformation ability of the composite interlayer were improved significantly after the multiple-steps rolling process. It is considered that the improvement of bonding quality was mainly attributed to the enhanced bonding strength due to the accumulation of plastic strain, and also the atomic interdiffusion at the interface promoted the metallurgical bonding between the layers as proved in Fig. 3.

Fig. 10 shows the RT tensile fracture morphologies at higher magnification after different ARB cycles. Generally, it can be seen lots of dimples with a large and deep size on the fracture surfaces for both the as-received Al–AlN and Al–Mg

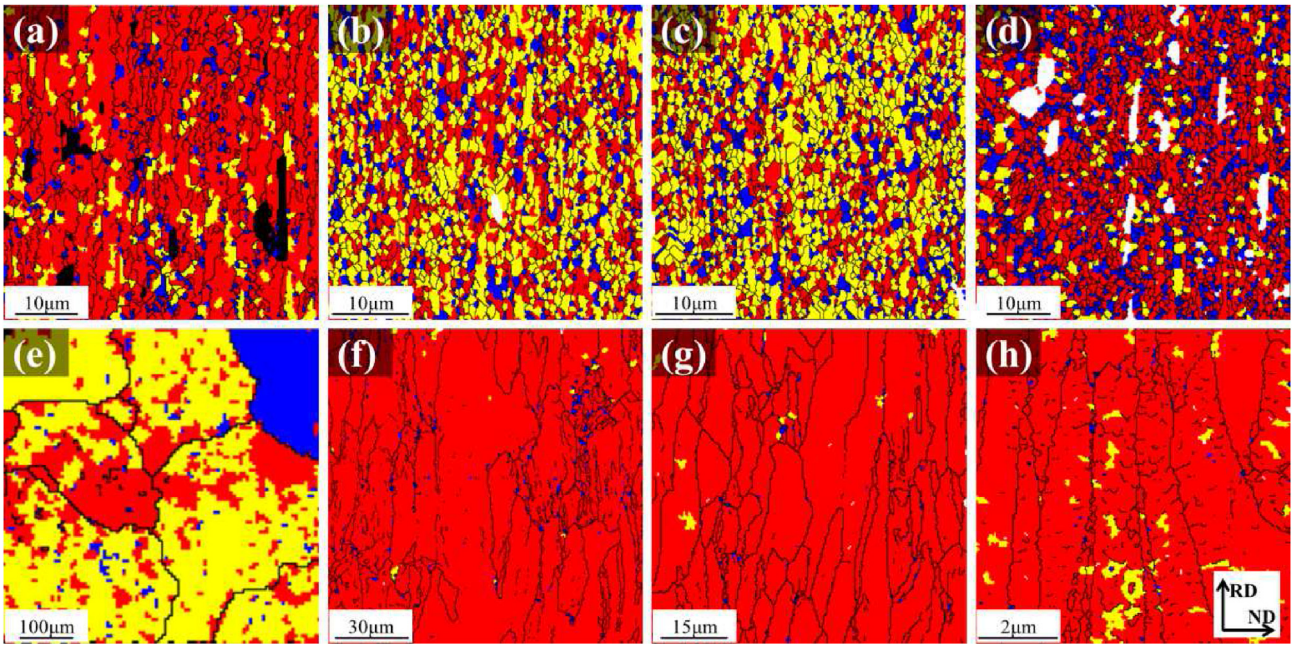

Fig. 12 – Recrystallized distribution illustrations (fully recrystallized grains are shown in blue, substructure grains in yellow, and severely deformed grains in red) of (a–d) Al–AlN layer and (e–h) Al–Mg layer in the laminated composite before and after ARB processing: (a, e) as-received; (b, f) one; (c, g) two; (d, h) three cycles.

(Fig. 10a and e), which are the typical ductile fracture characteristics. It is apparently that both the dimple size and depth are reduced significantly after the first ARB process (Fig. 10b and f). This is due to the matrix grains were refinement significantly and thus the work hardening rate has been reduced which caused the limited growth of the dimples. With increasing ARB cycle, there are no much variations on the dimple morphology and size for both the Al–AlN layer (Fig. 10c and d) and Al–Mg layer (Fig. 10g and h).

In order to investigate the tensile fracture behavior of the composite at cryogenic, the LNT tensile fracture surfaces of the composites were characterized. As shown in Fig. 11a, d and g, the tensile fracture morphologies of composites at lower magnification shows the same trend as that of RT tensile. It can be seen that there is a obvious crack distributed at the interface on the fracture surface for the composite after one ARB cycle, and the crack size reduced with the increase of ARB cycles. This indicates that the bonding strength and the synergistic deformation ability of the composite interlayer were improved after multiple roll bonding. At a higher magnification (Fig. 11b, e and h), a lot of small dimples (indicated by the yellow arrow) and a few

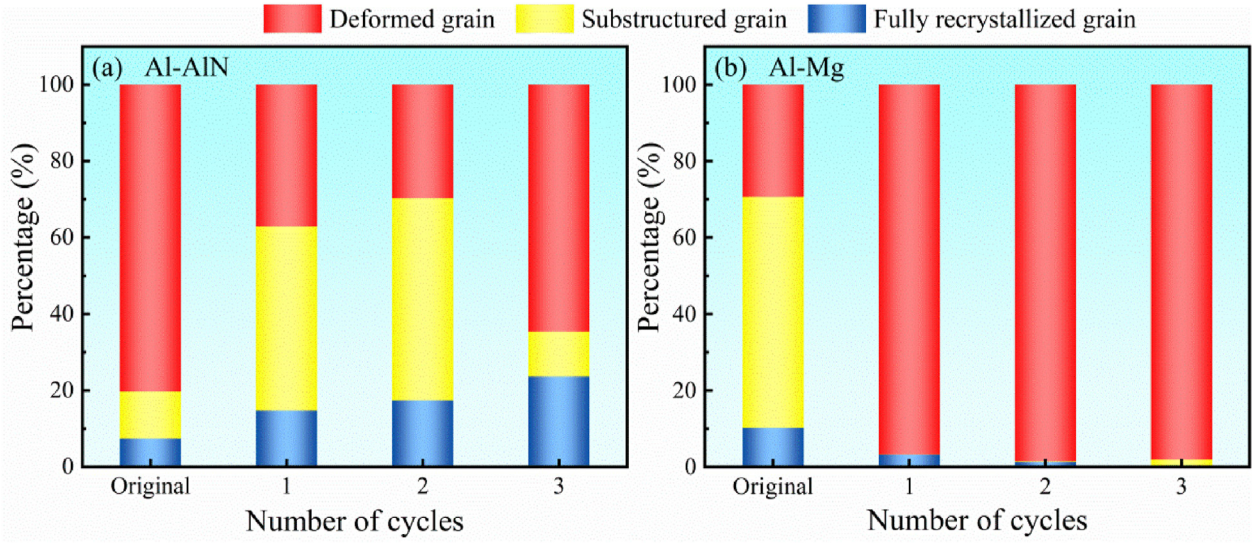

Fig. 13 – Recrystallization statistics of (a) Al–AlN layer and (b) Al–Mg layer in the laminated composite before and after ARB processing.

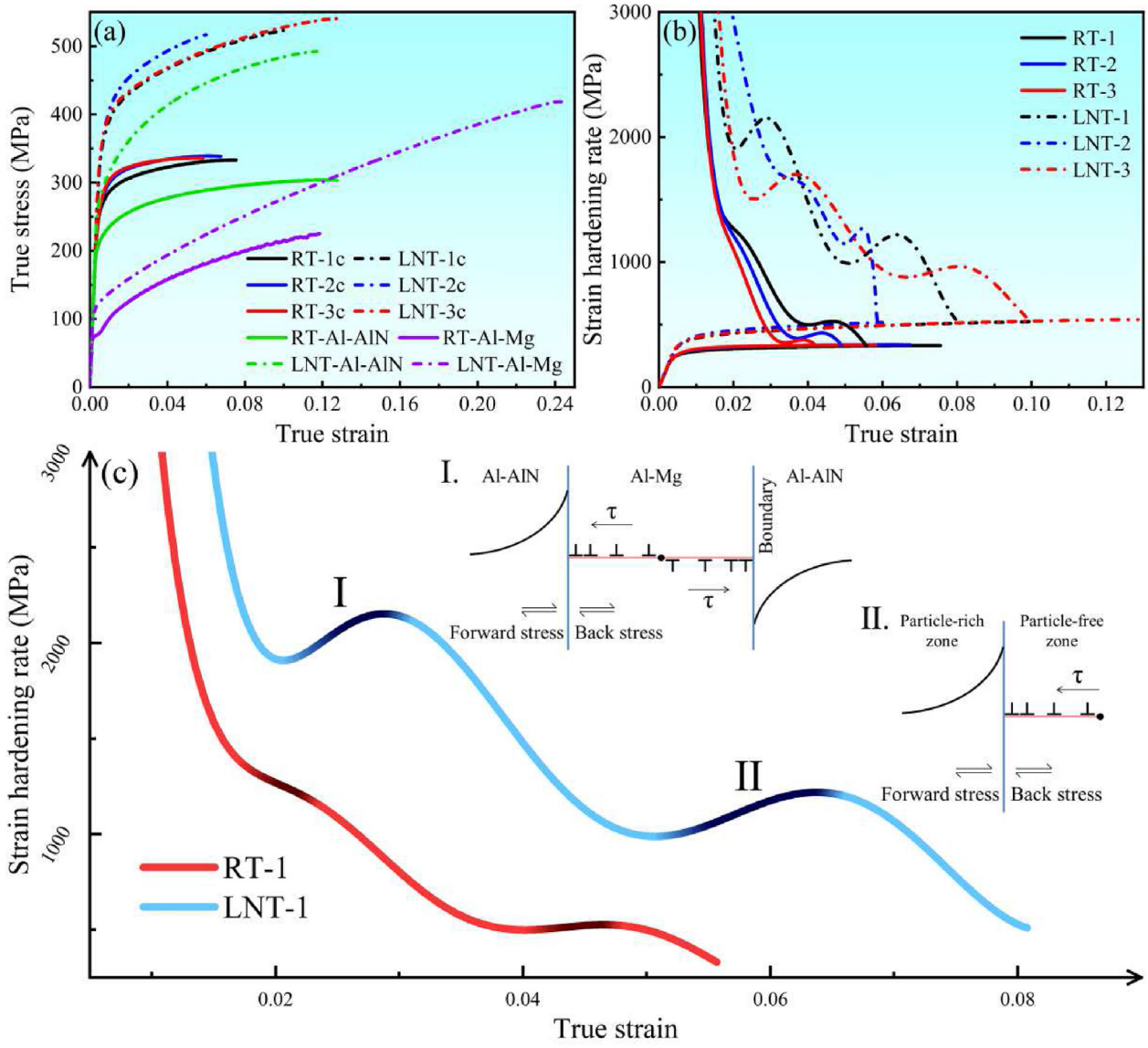

Fig. 14 – (a) True stress–strain curves of the Al–AlN/Al–Mg composite before and after ARB processing were tested at RT and LNT; (b) the corresponding strain hardening rate curves of ARB processed samples; (c) representative curve of the strain hardening curve and schematic of GNDs piling up.

large holes (indicated by the blue arrow) can be observed on the fracture surface of the Al–AlN layer. The formation of large holes may be due to the massive accumulation of dislocations around the AlN particle-rich zone at low temperatures and then crack initiated at the interface, which led to the debonding of the matrix and particles during the tensile deformation. It was shown that the distribution of AlN particles was gradually uniform with the increase of ARB cycles and then the number of large holes also decreased. As shown in Fig. 11c, there are rock candy patterns on the fracture surface of the Al–Mg layer (indicated by the red arrow) after the first ARB cycle, which are the typical intergranular fracture feature characteristics. Moreover, many dimples can be observed on the fracture surface, thus the Al–Mg layer is intergranular dimple fracture after the first ARB cycle. After two and three ARB cycles, a lot of dimples were observed on the fracture surface without obvious intergranular fracture, which were the typical ductile fracture characteristics. The transformation of the fracture form is due to grain refinement caused by the accumulation of plastic strain.

4. Discussion

4.1. *Deformation and recrystallization in Al–Mg/Al–AlN laminated composites*

The reasons for the different grain morphology changes of Al–AlN layer and Al–Mg layer after ARB processing were

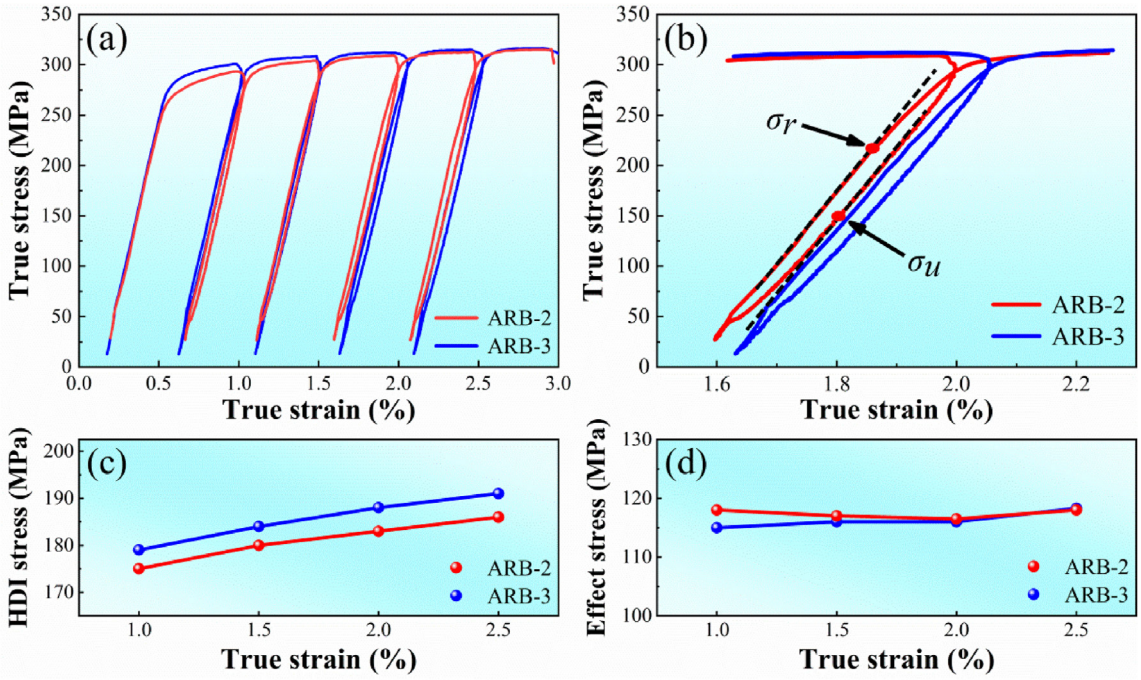

Fig. 15 – (a) LUR stress–strain curves of Al–AlN/Al–Mg composites with different cycles; (b) the 3rd measured hysteresis loop with σ_u and σ_r defined; (c) HDI stress and (d) effective mechanical stress varies with applied strain of Al–AlN/Al–Mg composites after different ARB cycles.

analyzed by statistical distribution of recrystallized grains in composites after different cycles. As shown in Fig. 12a, most are deformed grains in the microstructure of the as-received Al–AlN after extrusion deformation. After ARB processing, the Al–AlN layer was mainly composed of deformed grains and substructure grains, and the proportion of recrystallized grains gradually increasing to 24% after three cycles (Fig. 12b–d and Fig. 13a). During ARB processing, the continuous strain applied to the composite leads to a large number of dislocations within the grains of the Al matrix. The dislocations evolved and entangled with each other with the increasing strain, forming dislocation cells or dislocation walls and then further formed substructures, resulting in a high proportion of deformed grains and substructure grains in the Al–AlN layer. The interaction between AlN particles and dislocations further intensified the accumulation of dislocations in the matrix. When the strain was large enough, the grains undergo dynamic recovery and recrystallization during the roll bonding process. In addition, the intermediate preheating process before each rolling can also promote recrystallization to some extent. Both of the two effects lead to the increase of matrix grain size after the third ARB processing. As shown in Fig. 12f–h and Fig. 13b, the Al–Mg layer was mainly composed of deformed grains with a proportion of about 98% after ARB processing. Due to the coarse grains in the as-cast Al–Mg sample, their deformation ability and the ability to generate and accommodate dislocations were better than those in the Al–AlN layer during the ARB deformation process, thus a large number of deformed grains were generated without recrystallization.

4.2. *HDI strengthening effect in Al–AlN/Al–Mg laminated composites*

Traditionally, grain refinement can significantly increase the strength of alloys, but this is usually accompanied by the sacrifice of ductility. Tensile tests showed that the strength of the Al–AlN/Al–Mg composites increased significantly and the ductility was hardly decreased with the increase of ARB cycles. The true stress–strain curves and strain hardening rate curves of the laminated composite tested at RT and LNT after different ARB cycles are shown in Fig. 14a and b. The strain hardening rate is increased for all samples in the LNT tensile test compared to that in the RT tensile test, resulting in a significant increase in the ductility of the composite. It is found that there are two stages on the strain hardening curves of the heterostructured Al–Mg/Al–AlN laminated composite where the strain hardening rate hardly decreases or even increases (Fig. 14b), which is different from the strain hardening rate curve of traditional alloys.

Fig. 14c shows a representative curve of the strain hardening curve, including two distinct rising stages. The deformation process of the composites can be analyzed as following. Upon tensile loading, the soft Al–Mg layer yields firstly but could not deform freely due to the deformation constraint caused by the Al–AlN layer. In this elastic–plastic deformation stage, GNDs will be generated and accumulated at Al–AlN/Al–Mg interface, resulting in long-range back stress in Al–Mg grains. The back stress is directional and can counteract some applied shear stress. Therefore, this leads to Al–Mg layer exhibiting higher strength, which significantly

enhances the yield strength of the Al–AlN/Al–Mg composites [1]. The accumulation of GNDs at the interface will also exert forward stress on the grains in Al–AlN layer, which promoted their plastic deformation. When the tensile stress was further increased, the Al–AlN and Al–Mg layers co-deformed plastically and the soft Al–Mg grains underwent higher plastic strain, resulting in a strain gradient near the hetero-interface. That is to say, the strain gradient needs to be sustained by GNDs, resulting in the back stress in Al–Mg grains and the forward stress in Al–AlN grains, which collectively produce a hetero-deformation induced hardening at the *stage I*. Moreover, the difference in strength between the Al–AlN and Al–Mg layers at LNT is larger than that at RT, more GNDs can be accumulated at the interface and thus larger back stresses can be generated. Therefore, the *stage I* of the strain hardening curve measured at LNT has a more significant rise. For the *stage II*, the Al–AlN layer can be divided into hard and soft zones due to the non-uniform distribution of AlN particles in the Al matrix. During the tensile deformation, GNDs accumulated in the soft zone of the Al–AlN layer and generated back stress and forward stress, which leads to the rise of the *stage II* of the strain hardening curve. As the number of ARB cycles increases, the AlN particles were gradually distributed uniformly in the Al matrix, and thus the HDI hardening decreases and the strain hardening rate curve rise gradually decreases. In other words, it is the hetero-deformation that leads to the development of back stress and forward stress, which collectively produce the strengthening and extra work hardening [39].

Actually, the contribution of HDI stress to strength can be measured by Loading-Unloading-Reloading (LUR) testing. Fig. 15a shows the LUR test hysteresis loops measured at varying tensile strains after two and three ARB cycles. The HDI stress (σ_{HDI}) and effective mechanical stress (σ_{eff}) at different tensile strains can be calculated by Equations (2) and (3):

$$\sigma_{HDI} = \frac{\sigma_r + \sigma_u}{2} \tag{2}$$

$$\sigma_{eff} = \sigma_t - \sigma_{HDI} \tag{3}$$

where the σ_r and σ_u are the reloading yield stress and unloading yield stress (as indicated in Fig. 15b), the σ_t is the true stress. As shown in Fig. 15c, the HDI stress increased with strain, which is due to the enhanced accumulation of GNDs at the hetero-interface during the tensile test. Moreover, the effective mechanical stress of the sample was almost unchanged after the second and third ARB cycles (Fig. 15d), but the HDI stress was higher due to the fact that more heterogeneous interfaces could accumulate more GNDs during the tensile deformation, which contribute to the higher strength after three ARB cycles.

5. Conclusions

In this work, a heterostructured Al–AlN/Al–Mg laminated composite was successfully fabricated by ARB processing to improve the combination of tensile strength and ductility synergistically. The microstructure, mechanical properties and HDI stress strengthening mechanism of the laminated composites were investigated. The conclusions can be summarized as follows:

(1) The interfaces in the Al–AlN/Al–Mg laminated composites were well bonded and remained straight up to three ARB cycles. The bonding quality of the laminated interface was improved significantly based on the atomic interdiffusion with the increase of ARB cycles.
(2) The Al matrix grains in the Al–AlN/Al–Mg laminated composites were refined significantly, especially the average grain size in Al–Mg layer decreased from lager than 220 μm to smaller than 2.19 μm. While the Al grains in the Al–AlN composite were refined to the ultrafine grain regime firstly during the first two cycles and increased slight to 1.33 μm after the third cycle due to recrystallization. Meanwhile, the distribution of AlN particles becomes more uniform and more dislocations entangled and accumulated around the particles after the ARB processing.
(3) The microhardness and tensile strength of the composites increased significantly after ARB processing without obvious sacrifice of ductility. The microhardness of Al–AlN and Al–Mg layers increased to 91.3 HV and 106.7 HV after three ARB cycles, respectively. Compared with the room temperature tensile properties, the cryogenic UTS, YS and UE of the Al–AlN/Al–Mg composite under liquid nitrogen temperature were reached to 473.7 MPa, 363.1 MPa and 9.88%, increased by 51.8%, 39.0% and 83.3%, respectively. The strain hardening rate at liquid nitrogen temperatures was also significantly improved.
(4) It is revealed that the HDI stress contributed significantly to the strain hardening and strength increase of the composites because of the accumulation of GNDs at the hetero-interfaces. Due to the accumulation of GNDs between the Al–AlN and Al–Mg layers and between the AlN particle-rich and particle-free zones in the Al–AlN layer, there are two distinct strengthening stages in the strain hardening curve of the composite. In addition, the HDI stress strengthening was also enhanced with the increase of ARB cycles due to the fact that more heterogeneous interfaces are benefit to the accumulation of more GNDs during the deformation.

CRediT authorship contribution statement

Xinda Sun: Investigation, Writing-original draft, Writing-review & editing. **Xiaojie Hao:** Investigation. **Jinfeng Nie:** Conceptualization, Funding acquisition, Supervision, Writing – review & editing. **Yong Fan:** Data analysis. **Yuyao Chen:** Data analysis. **Sida Liu:** Writing-review & editing. **Xiangfa Liu:** Supervision. **Yonghao Zhao:** Supervision, Writing – review & editing.

Data availability

All data included in this study are available upon request by contact with the corresponding author.

Declaration of Competing Interest

The authors declare that they have no known competing financial interests or personal relationships that could have appeared to influence the work reported in this paper.

Acknowledgements

The authors are grateful to the National Natural Science Foundation of China (Nos. 52071179, 52271033 and 51731007) and the Fundamental Research Funds for the Central Universities (Nos. 30920021160 and 30919011405).

REFERENCES

[1] Wu X, Zhu Y. Heterogeneous materials: a new class of materials with unprecedented mechanical properties. Mater Res Lett 2017;5(8):527–32. https://doi.org/10.1080/21663831.2017.1343208.

[2] Huang CX, Wang YF, Ma XL, Yin S, Höppel HW, Göken M, et al. Interface affected zone for optimal strength and ductility in heterogeneous laminate. Mater Today Off 2018;21(7):713–9. https://doi.org/10.1016/j.mattod.2018.03.006.

[3] Nie JF, Chen YY, Chen X, Liu XF, Liu GL, Zhao YH, et al. Stiff, strong and ductile heterostructured aluminum composites reinforced with oriented nanoplatelets. Scripta Mater 2020;189:140–4. https://doi.org/10.1016/j.scriptamat.2020.08.017.

[4] Wang YF, Wei YG, Zhao ZF, Long H, Lin ZY, Guo FJ, et al. Activating dispersed strain bands in tensioned nanostructure layer for high ductility: the effects of microstructure inhomogeneity. Int J Plast 2022;149:103159. https://doi.org/10.1016/j.ijplas.2021.103159.

[5] Gu L, Liang NN, Chen YY, Zhao YH. Achieving maximum strength-ductility combination in fine-grained Cu-Zn alloy via detwinning and twinning deformation mechanisms. J Alloys Compd 2022;906:164401. https://doi.org/10.1016/j.jallcom.2022.164401.

[6] Ma XL, Huang CX, Xu WZ, Zhou H, Wu XL, Zhu YT. Strain hardening and ductility in a coarse-grain/nanostructure laminate material. Scripta Mater 2015;103:57–60. https://doi.org/10.1016/j.scriptamat.2015.03.006.

[7] Fang XT, Li ZK, Wang YF, Ruiz M, Ma XL, Wang HY, et al. Achieving high hetero-deformation induced (HDI) strengthening and hardening in brass by dual heterostructures. J Mater Sci Technol 2022;98:244–7. https://doi.org/10.1016/j.jmst.2021.03.088.

[8] Wu XL, Zhu YT, Lu K. Ductility and strain hardening in gradient and lamellar structured materials. Scripta Mater 2020;186:321–5. https://doi.org/10.1016/j.scriptamat.2020.05.025.

[9] Zhu YT, Ameyama K, Anderson PM, Beyerlein IJ, Gao HJ, Kim HS, et al. Heterostructured materials: superior properties from hetero-zone interaction. Mater Res Lett 2021;9(1):1–31. https://doi.org/10.1080/21663831.2020.1796836.

[10] Wu XL, Yang MX, Yuan FP, Wu GL, Wei YJ, Huang XX, et al. Heterogeneous lamella structure unites ultrafine-grain strength with coarse-grain ductility. Proc. Natl. Acad. Sci. U.S.A 2015;112(47):14501–5. https://doi.org/10.1073/pnas.1517193112.

[11] Wang YF, Wei YG, Zhao ZF, Lin ZY, Guo FJ, Cheng Q, et al. Mechanical response of the constrained nanostructured layer in heterogeneous laminate. Scripta Mater 2022;207:114310. https://doi.org/10.1016/j.scriptamat.2021.114310.

[12] Huang JX, Liu Y, Xu T, Chen XF, Lai QQ, Xiao LR, et al. Dual-phase hetero-structured strategy to improve ductility of a low carbon martensitic steel. Mater Sci Eng, A 2022;834:142584. https://doi.org/10.1016/j.msea.2021.142584.

[13] Moering J, Ma XL, Malkin J, Yang MX, Zhu YT, Mathaudhu S. Synergetic strengthening far beyond rule of mixtures in gradient structured aluminum rod. Scripta Mater 2016;122:106–9. https://doi.org/10.1016/j.scriptamat.2016.05.006.

[14] Zhu YT, Wu XL. Perspective on hetero-deformation induced (HDI) hardening and back stress. Mater Res Lett 2019;7(10):393–8. https://doi.org/10.1080/21663831.2019.1616331.

[15] Li ZK, Fang XT, Wang YF, Jiang P, Wang JJ, Liu CM, et al. Tuning heterostructures with powder metallurgy for high synergistic strengthening and hetero-deformation induced hardening. Mater Sci Eng, A 2020;777:139074. https://doi.org/10.1016/j.msea.2020.139074.

[16] Liu YF, Cao Y, Mao QZ, Zhou H, Zhao YH, Jiang W, et al. Critical microstructures and defects in heterostructured materials and their effects on mechanical properties. Acta Mater 2020;189:129–44. https://doi.org/10.1016/j.actamat.2020.03.001.

[17] Xia YP, Wu H, Miao KS, Li X, Xu C, Geng L, et al. Effects of the layer thickness ratio on the enhanced ductility of laminated aluminum. J Mater Sci Technol 2022;111:256–67. https://doi.org/10.1016/j.jmst.2021.08.093.

[18] Wang YF, Yang MX, Ma XL, Wang MS, Yin K, Huang AH, et al. Improved back stress and synergetic strain hardening in coarse-grain/nanostructure laminates. Mater Sci Eng, A 2018;727:113–8. https://doi.org/10.1016/j.msea.2018.04.107.

[19] Ghasali E, Pakseresht A, Safari-kooshali F, Agheli M, Ebadzadeh T. Investigation on microstructure and mechanical behavior of Al–ZrB_2 composite prepared by microwave and spark plasma sintering. Mater Sci Eng A 2015;627:27–30. https://doi.org/10.1016/j.msea.2014.12.096.

[20] Rath AP, Patel SK, Deep N. Synthesis and characterisation of silicon carbide nanoparticulate reinforced metal matrix composite. Mater Today Proc 2020;33:5419–24. https://doi.org/10.1016/j.matpr.2020.03.136.

[21] Nie JF, Liu YF, Wang F, Zhou H, Cao Y, Liu XF, et al. Key roles of particles in grain refinement and material strengthening for an aluminum matrix composite. Mater Sci Eng, A 2021;801:140414. https://doi.org/10.1016/j.msea.2020.140414.

[22] Xu ZB, Roven HJ, Jia ZH. Mechanical properties and surface characteristics of an AA6060 alloy strained in tension at cryogenic and room temperature. Mater Sci Eng, A 2015;648:350–8. https://doi.org/10.1016/j.msea.2015.09.083.

[23] Su LH, Deng GY, Luzin V, Wang H, Wang ZY, Yu HL, et al. Effect of cryogenic temperature equal channel angular pressing on microstructure, bulk texture and tensile properties of AA1050. Mater Sci Eng, A 2020;780:139190. https://doi.org/10.1016/j.msea.2020.139190.

[24] Park JH, Kim SH, Kim SG, Kim HW, Lee JC. Improved cryogenic properties of the Al-xMg alloys enabled by twin-roll strip casting. J Mater Res Technol 2021;13:1285–95. https://doi.org/10.1016/j.jmrt.2021.05.025.

[25] Ma X, Zhao YF, Xie KW, Liu XF. Microstructure evolution and high temperature tensile properties of AlNp/Al–Fe composites induced by microalloying. J Alloys Compd 2019;786:1005–12. https://doi.org/10.1016/j.jallcom.2019.02.069.

[26] Saito Y, Utsunomiya H, Tsuji N, Sakai T. Novel ultra-high straining process for bulk materials—development of the accumulative roll-bonding (ARB) process. Acta Mater 1999;47(2):579–83. https://doi.org/10.1016/S1359-6454(98)00365-6.
[27] Xu RR, Liang NN, Zhuang LM, Wei DJ, Zhao YH. Microstructure and mechanical behaviors of Al/Cu laminated composites fabricated by accumulative roll bonding and intermediate annealing. Mater Sci Eng, A 2022;832:142510. https://doi.org/10.1016/j.msea.2021.142510.
[28] Hosseini M, Pardis N, Danesh Manesh H, Abbasi M, Kim DI. Structural characteristics of Cu/Ti bimetal composite produced by accumulative roll-bonding (ARB). Mater Des 2017;113:128–36. https://doi.org/10.1016/j.matdes.2016.09.094.
[29] You CP, Xie WB, Miao S, Liang TX, Zeng LF, ZhangXH, et al. High strength, high electrical conductivity and thermally stable bulk Cu/Ag nanolayered composites prepared by cross accumulative roll bonding. Mater Des 2021;200:109455. https://doi.org/10.1016/j.matdes.2021.109455.
[30] Jamaati R, Toroghinejad MR. Application of ARB process for manufacturing high-strength, finely dispersed and highly uniform Cu/Al2O3 composite. Mater Sci Eng, A 2010;527(27):7430–5. https://doi.org/10.1016/j.msea.2010.08.038.
[31] Jamaati R, Amirkhanlou S, Toroghinejad MR, Niroumand B. Effect of particle size on microstructure and mechanical properties of composites produced by ARB process. Mater Sci Eng, A 2011;528(4):2143–8. https://doi.org/10.1016/j.msea.2010.11.056.
[32] Wu CC, Gao T, Nie JF, Jiang L, Liu XF. In-situ synthesis of nano SiC particles in Al–Si–C system at 750 °C. J Mater Res Technol 2021;13:716–26. https://doi.org/10.1016/j.jmrt.2021.05.008.
[33] Gao T, Bian YH, Liu XF. Strengthening behavior of nano–particle networks in an in–situ synthesized (α–Al_2O_3 + ZrB_2)/Al composite. Mater Lett 2021;301:130309. https://doi.org/10.1016/j.matlet.2021.130309.
[34] Gao T, Liu LY, Song JP, Liu GL, Liu XF. Synthesis and characterization of an in-situ Al_2O_3/Al–Cu composite with a heterogeneous structure. J Alloys Compd 2021;868:159283. https://doi.org/10.1016/j.jallcom.2021.159283.
[35] Yang SC, Cui CX, Cui S, Liu SJ. Ti–46Al–4Nb alloy refined and reinforced by in-situ TiC nanoparticles and TiB_2 whiskers. J Alloys Compd 2022;892:162195. https://doi.org/10.1016/j.jallcom.2021.162195.
[36] Ma X, Zhao YF, Tian WJ, Qian Z, Chen HW, Wu YY, et al. A novel Al matrix composite reinforced by nano-AlNp network. Sci Rep 2016;6(1):34919. https://doi.org/10.1038/srep34919.
[37] Kümmel F, Kreuz M, Hausöl T, Höppel HW, Göken M. Microstructure and mechanical properties of accumulative roll-bonded AA1050A/AA5005 laminated metal composites. Metals 2016;6(3):56. https://doi.org/10.3390/met6030056.
[38] Lee JM, Lee BR, Kang SB. Control of layer continuity in metallic multilayers produced by deformation synthesis method. Mater Sci Eng, A 2005;406(1):95–101. https://doi.org/10.1016/j.msea.2005.06.030.
[39] Shi P, Zhong Y, Li Y, Ren W, Zheng T, Shen Z, et al. Multistage work hardening assisted by multi-type twinning in ultrafine-grained heterostructural eutectic high-entropy alloys. Mater Today 2020;41:62–71. https://doi.org/10.1016/j.mattod.2020.09.029.